Adjustable Ellipsoid Nanoparticles Assembled from Re-engineered Connectors of the Bacteriophage Phi29 DNA Packaging Motor

Feng Xiao,[†,⊥] Ying Cai,[†,⊥,¶] Joseph Che-Yen Wang,[‡] Dominik Green,[‡] R. Holland Cheng,[‡] Borries Demeler,[§] and Peixuan Guo[†,*]

[†]Department of Biomedical Engineering, College of Engineering and College of Medicine, University of Cincinnati, Cincinnati, Ohio 45221, [‡]Department of Molecular & Cellular Biology, University of California, Davis, California 95616, and [§]Department of Biochemistry, The University of Texas Health Science Center at San Antonio, 7703 Floyd Curl Drive, San Antonio, Texas 78229. [⊥]Co-first-author. [¶]Current address: VGX Pharmaceuticals, Inc, 2700 Research Forest Drive, Suite 180, The Woodlands, Texas 77381.

ABSTRACT A 24 × 30 nm ellipsoid nanoparticle containing 84 subunits or 7 dodecamers of the re-engineered core protein of the bacteriophage phi29 DNA packaging motor was constructed. Homogeneous nanoparticles were obtained with simple one-step purification. Electron microscopy and analytical ultracentrifugation were employed to elucidate the structure, shape, size, and mechanism of assembly. The formation of this structure was mediated and stabilized by N-terminal peptide extensions. Reversal of the 84-subunit ellipsoid nanoparticle to its dodecamer subunit was controlled by the cleavage of the extended N-terminal peptide with a protease. The 84 outward-oriented C-termini were conjugated with a streptavidin binding peptide which can be used for the incorporation of markers. This further extends the application of this nanoparticle to pathogen detection and disease diagnosis by signal enhancement.

KEYWORDS: nanobiotechnology · bionanotechnology · viral DNA packaging · phi29 DNA packaging motor · protein nanoparticles · virus assemble · bacteriophage phi29 connector

Rational design of nanoparticles has become a prevalent trend requiring an in-depth comprehension of the chemical and physical characteristics of their building blocks. Taking advantage of the highly specific binding properties of biomolecules, the combination of biotechnology and nanotechnology has led to the development of hybrid nanobiomaterials. Biological materials, in the form of DNA, RNA, protein, and lipids, serve as models for the self-recognition and self-assembly of bionanoparticles.[1−3] Peptides also play a unique role in nanostructure design, owing to their diversity, simplicity of synthesis, and ease of modifying them for a variety of functions. Understanding the self-assembly mechanism of these biomaterials enables us to design and engineer biomimetics on a nanoscale. Extensive investigations have been conducted and successful applications achieved with DNA,[2,4] RNA,[3,5−9] viral proteins,[10−13] bacterial S-layer proteins,[14−16] peptides, and peptidomimetics.[17]

Bacteriophage phi29 is one of several well-studied, small-tailed phages. It infects *Bacillus subtilis*. This double-stranded DNA virus utilizes a unique motor to package its 19.3 kb genome into a preformed procapsid.[18] The connector protein is an essential component in the phi29 DNA-packaging motor. Its crystal structure, determined at high-resolution, is a 12-fold symmetric dodecamer that forms a truncated cone with a length of 7.5 nm, a diameter of 13.8 nm at the wide end and 6.8 nm at the narrow end, and contains a 3.6 nm central pore for DNA translocation.[19,20] A crystal structure failed to reveal the N-terminal 13 amino acids because of their flexibility in structure. Inclusion of these 13 amino acid at the N-terminus of each wild-type gp10 subunit results in about 7.8 nm in diameter at the narrow end of the connector.[12]

Connector proteins of the bacteriophage phi29 can assemble into a rosette-like particle after interaction with pRNA.[12,21,22] In this study, we report the construction of a distinct globular nanoparticle assembled from a re-engineered phi29 connector protein. The maximum diameter of the resultant nanoparticles is twice as large as the maximum diameter of the connector formed by native connector protein gp10, in addition to having a vastly different quaternary assembly. The structural transition between the connector and the nanoparticle can be easily controlled *via* the addition

*Address correspondence to guopn@ucmail.uc.edu.

Received for review February 24, 2009 and accepted July 07, 2009.

Published online July 17, 2009.
10.1021/nn900187k CCC: $40.75

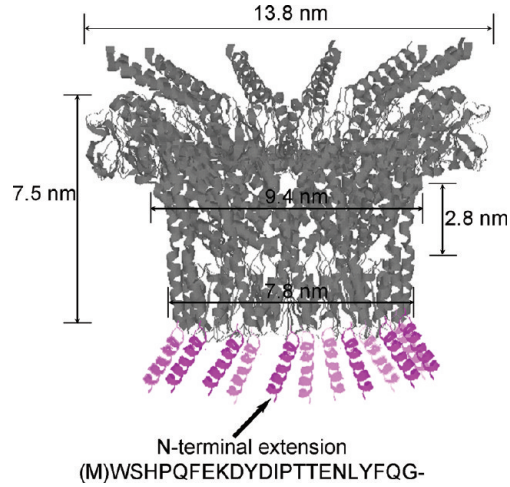

Figure 1. Illustration of the construct of N-Strep connector with N-terminal extension in side view. Computer modeling of the connector was presented in full sequence. The diameter of about 7.8 nm at the narrow end illustrates the wild-type connector that includes the 13 amino acid at the N-terminus.[12] The 22-residue extension on the N-terminus was shown in magenta.

or removal of the N-terminal peptide. This globular nanoparticle, with a surface exposed tag for functional conjugation with other molecules, has potential applications in nanotechnology.

RESULTS

Addition of the N-Terminal Peptide Produced a Novel Globular Nanoparticle. A 22-residue peptide was used to extend the N-terminus of gp10 protein of the phi29 connector, resulting in a modified N-Strep connector. This peptide included a Streptavidin binding peptide (WSHPQFEK, referred to as "Strep-II tag")[23,24] and a tobacco etch virus (TEV) protease cleavage site (ENLYFQG) (Figure 1). The Strep-tag, which bound the streptavidin protein, facilitated one-step Strep-Tactin (IBA GmbH, Germany) purification of protein,[25] while the TEV protease cleavage-site enabled removal of the peptide when necessary. The purified N-Strep connector particles, first examined by transmission electron microscopy (TEM) (Figure 2A), revealed drastically different projections than typically isolated wild-type connectors, which form a dodecameric structure with a diameter of 7.8 nm at the narrow end[12] and 13.8 nm at the wider end[19,20] (Figure 1). However, the nanoparticles formed by the N-strep connector, which displayed an ellipsoid shape (see section on imaging the N-strep nanoparticles) were 30 nm (transverse, major axis) by 24 nm (lengthwise, minor axis), displaying a 5- or 10-fold rotational symmetry.

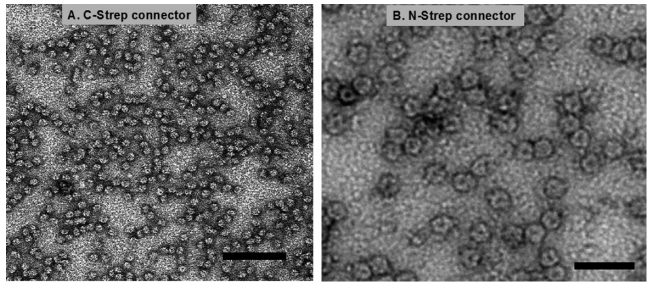

Figure 2. TEM micrographs of (A) C-strep connector and (B) N-strep connector, ellipsoid nanoparticles. Bar = 100 nm.

Switching between Connector and the Ellipsoid Nanoparticle by Cleaving the N-Terminal Peptide with Proteinase. The N-Strep connector protein preferentially assembles into ellipsoid nanoparticles within the cell during expression or within the crude lysate. These particles were purified to homogeneity since they were fairly stable under a range of salt concentrations, pH, and temperature. A TEV enzyme recognition site was inserted between the connector and the N-terminal extended peptide to allow the added peptide to be removed by protease treatment. Removal of the N-terminal peptide by TEV protease resulted in the dissociation of the ellipsoid particles into individual connectors, as revealed by TEM imaging. Gradient sedimentation with 15−35% glycerol further confirmed the similarity in the sedimentation rate of the TEV-processed particle and individual connectors (Figure 3). The N-Strep connector primarily centered at fraction 9 of 29 total fractions (Figure 3, dot line). However, removal of the N-terminus tag *via* TEV cleavage caused the peak to shift to fraction 25 where the wild-type dodecamer connectors can be found (Figure 3, solid line with open circle). These results suggest that adding the 22-residue peptide to the N-terminus of the connector contributes to the assembly of particles that are different from individual connectors in size, conformation, and mass, and subsequent removal of the N-terminus tag leads to dissociation of the nanoparticle.

Mass and Shape Analysis *via* Sedimentation Velocity by Analytical Ultracentrifugation Revealed Nanoparticles with Seven Connectors or 84 Copies of Monomeric gp10. Sedimentation velocity (SV) experiments can be used to estimate the molecular weight, partial concentration, and relative shape of multiple solutes in a mixture of macromolecules.[26] A van Holde−Weischet analysis[27] provides diffusion corrected sedimentation distributions and can be used to ascertain composition. Shape and molecular weight (MW) are derived from the sedimentation (s) and diffusion (D) coefficients fitted in the finite element solutions of the Lamm equation[28] implemented in the 2-dimensional spectrum analysis (2DSA) or genetic algorithm (GA) analysis, and from the knowledge of the partial specific volume. Shape is parametrized with the frictional ratio, f/f_0, a measurement of the globularity of the solute. An f/f_0 value of 1.0 refers to a spherical particle, while values larger than 2.5 generally indicate a nonglobular, unfolded or extended, or chainlike molecule, such as DNA or fibrils. Values between 1.2−1.4 are typical for moderately globular proteins. The partial specific volume was estimated from the protein sequence to be 0.7265 cm^3/g for both the N-Strep connector and the C-strep connector. The C-strep

connector without N-terminus modification serves as a single connector control. A van Holde−Weischet sedimentation coefficient distribution indicated that N-Strep connectors are present as a mixture of three predominant species: 78.00 S (42%), 15.04 S (38%) and 3.72 S (20%), while N-terminal unmodified proteins, C-Strep connector, were homogeneous at 15.14 S (100%) (Figure 4). To further investigate the identity of the three peaks, a GA−MC (genetic algorithm−Monte Carlo) analysis[29,30] was performed. This analysis can resolve a mixture of solutes according to size and shape, and provide partial concentrations for each species. Results are presented as plots of s vs f/f_0. Partial concentration is measured in optical density units and is represented as a color gradient. The GA−MC analysis for C-Strep connector is shown in Figure 5, the same analysis for N-Strep connector is shown in Figure 6. Confidence intervals for sedimentation and diffusion coefficients, frictional ratios, partial concentration, and molecular weight of each species are summarized for the N-Strep connectors in Table 1 and the C-Strep connectors in Table 2. The MWs were consistent with monomeric (protein gp10), 12-meric (connector), and 84-meric (the ellipsoid nanoparticle) N-Strep connector. The f/f_0 values indicated an overall increase in globular shape from a monomeric unit to an 84-mer. An f/f_0 value of 1.1 (most globular) was determined for the 84-mer (seven dodecameric connectors), an f/f_0 value of 1.51 was determined for the dodecamer connector, and an f/f_0 value of 1.63 was determined for the monomeric protein gp10 subunit. The 12-mer dodecamer connector structure for the N-terminal unmodified nanoparticles, C-strep connector, was found to have an f/f_0 value of 1.38—similar to the frictional ratio obtained for the 12-mer of N-Strep connectors. The data agreed with the available information for the molecules and assemblies: protein gp10 is a linear molecule mainly composed of α-helix; the connector is a truncated cone shape structure with a 3.6 nm central channel, and the resulting nanoparticle has an ellipsoid shape, which shows a more globular conformation (as detailed in the next section).

Imaging the N-Strep Nanoparticles. It appears that most nanoparticles formed by N-strep connector within the data set exist as top-view only projections, since very few 2-fold symmetric side views could be detected (Figure 2B). Particles were found to preferentially lie along the major axis (transverse) as opposed to the minor axis (lengthwise). This finding, that the majority of particles displayed a size that corresponded to the major axis, supports the conclusion of the ellipsoid configuration (Figure 7). Each circular projection contains 10 arms of density that emanate radially outward from the particle center, suggesting the presence of a 10-fold symmetry axis. The length of each arm is approximately equivalent, all measuring between 7−9 nm in length. Additionally, nearly all of these projections contain a

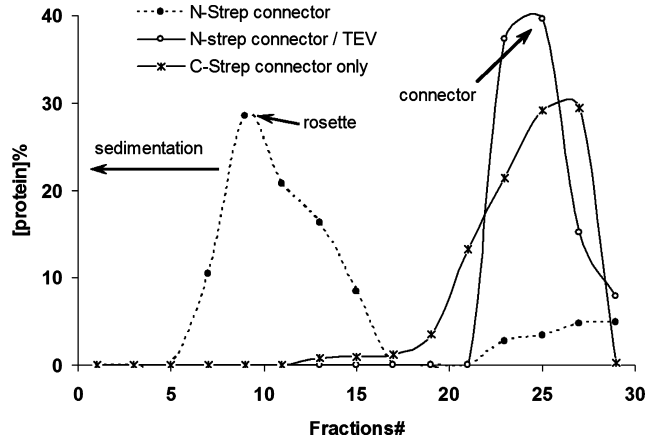

Figure 3. The 15−35% glycerol gradient sedimentation for C-strep connectors and N-strep connectors.

central ring of density from which the 10 radial arms extend. Within this central ring is a density-void pore measuring 3−4 nm in diameter, while the outermost diameter of the ring measures between 13−15 nm. The reprojection of the density of a modeled connector oriented perpendicular to its 12-fold axis measures ~8 nm along its edge, similar to that of the nanoparticle radial extension length. Also, the reprojection of a connector volume viewed down its 12-fold axis has a maximum diameter of 13.5 nm and a central pore measuring 3.5 nm in diameter. Both values match well with those determined for the nanoparticle central ring density. The projection image in Figure 7A has a measured length of 30 nm and a height of 24 nm. The length of this projection corresponds well to the maximum diameter of the nanoparticle projection (Figure 7B), suggesting that the view in Figure 7A corresponds to a projec-

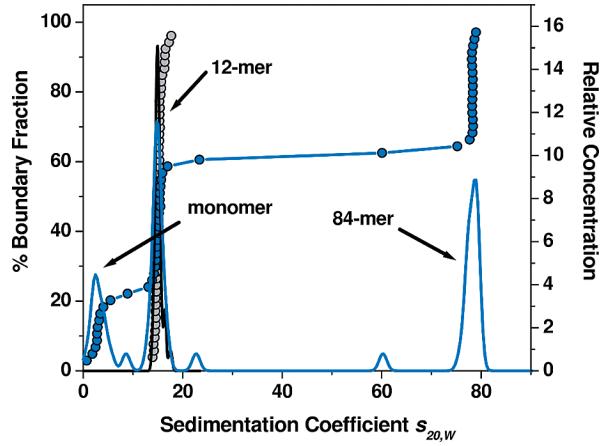

Figure 4. van Holde−Weischet analysis of C-strep connector (black) and N-Strep connector (blue). Integral distributions are shown as filled circles, and the percent boundary fraction is represented on the left *Y*-axis. Differential distributions of the same data are shown as solid lines, with relative concentration (unitless) shown in the right *Y*-axis. The C-strep connector is visible as a homogeneous species, sedimenting with a value of 15.14 S (100%), corresponding to a dodecamer of the connector. The N-Strep connector sediments as 3 distinct major species, 84-mer at 78.00 S (42.00%), 12-mer at 15.04 S (38.00%) and monomer gp10 at 3.72 S (20.00%).

TABLE 1. Genetic Algorithm—Monte Carlo Results for Three Major Species in N-Strep Nanoparticles

species	N-Strep, gp10 (monomer)	N-Strep connector (12-mer)	N-Strep ellipsoid particle (84-mer)
sedimentation coefficient ($\times 10^{-13}$ s)	2.46(2.45,2.47)	15.16(15.07,15.20)	78.11(77.95,78.31)
diffusion coefficient ($\times 10^{-7}$ cm/sec^2)	6.01(5.94,6.06)	2.74(2.66,2.77)	1.93(1.73,2.07)
frictional ratio	1.63(1.62,1.64)	1.51(1.49,1.53)	1.10(1.04,1.18)
molecular weight (kilodalton)	36.3(36.0,36.8)	493.8(485.4,503.7)	3590 (3329, 3985)
molecular weight (theor.) (kilodalton)	38.6	463.3	3243
partial concentration (optical density, 230 nm)	0.294(0.293,0.295)	0.489(0.479,0.496)	0.586(0.572,0.603)

tion orthogonal to that of Figure 7B. From these measurements, it is likely that the apparent 10-fold rotational symmetry of these projections arises from a circular array of five equatorial connectors arranged on their sides, with their narrow end facing inward. Two additional polar connectors, one above the equatorial connector axis and one below, attach narrow-end-first to the large central pore created by the association of the five equatorial connectors (Figure 7C). As seen from top, this nanoparticle configuration is expected to possess 5-fold rotational symmetry (although the view was not discernible from a 10-fold symmetry due to a low signal-to-noise ratio). Additionally, the side view projection of a nanoparticle (Figure 7A) reveals a horizontal mirror axis which suggests the presence of two polar connectors (one above and one below the equatorial connector plane) (Figure 7C). This yields a side dimension of 24 nm and an equatorial diameter of 30 nm (Figure 7A,C). Moreover, the vertical mirror axis suggests a view down the local 12-fold axis of an axial connector.

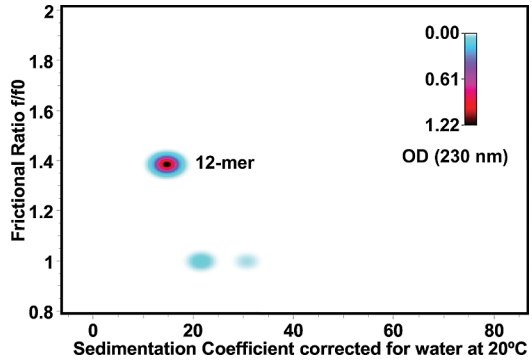

Figure 5. Genetic algorithm—Monte Carlo analysis: Frictional ratio *vs* sedimentation coefficient for C-strep connector. This plot shows the globularity (as parametrized by the frictional ratio, see text) plotted against sedimentation coefficient. The relative concentration of each species is shown in a color gradient ranging from white (zero concentration) to black (1.43 optical density units) measured at 230 nm. Only one major species is apparent (the second and third unlabeled species are negligible contaminants).

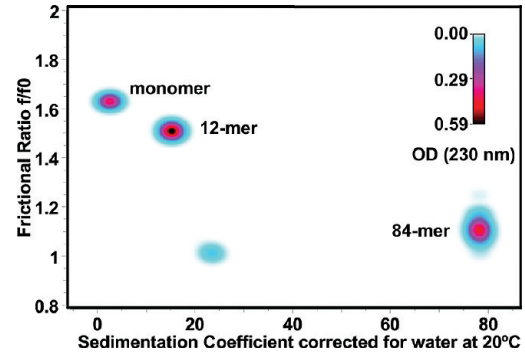

Figure 6. Genetic algorithm—Monte Carlo analysis: Frictional ratio *vs* sedimentation coefficient for N-strep connector. This plot shows the globularity (as parametrized by the frictional ratio, see text) plotted against sedimentation coefficient. The relative concentration of each species is shown in a color gradient ranging from white (zero concentration) to black (0.7 optical density units) measured at 230 nm. Three major species are apparent (the fourth, unlabeled species is a negligible contaminant). Molecules become increasingly globular when oligomerizing from monomer to 84-mer *via* 12-mer.

To further define the symmetry of the nanoparticles, rotational averaging was applied to each projection image. Application of n-fold rotational symmetry—n = 2, 5, and 10—to a single, well-resolved nanoparticle top-view resulted in the images depicted in Figure 7B. Although the imposition of rotational averaging generated images that closely resemble their parent projection, the image with imposed 5-fold rotational symmetry most accurately matches the structural interpretation of the nanoparticle described above. The 10-fold symmetry of individual nanoparticles seen within the data set most likely arises from the low signal-to-noise levels present in TEM imaging, thus causing the separation between individual equatorial connectors to be more difficult to resolve. The 2-fold rotational averaging mimics the 10-fold-imposed situation by simulating the superposition of a 36° rotation, inherently smearing the separation between neighboring connectors. The 2-fold symmetry was also applied to the side-view projection (Figure 7A). Enhancing the centralized equatorial connector hole and maintaining the same dimensions and relative pixel intensity measurements strongly support that a 2-fold symmetry (Figure 7A) is an accurate representation of the side-view (10-fold symmetry) projection depicted in Figure 7B.

TABLE 2. Genetic Algorithm—Monte Carlo Results for Single Component in C-Strep Nanoparticles

species	N-terminal unmodified connector (12-mer)
sedimentation coefficient ($\times 10^{-13}$ s)	14.61(14.60,14.62)
diffusion coefficient ($\times 10^{-7}$ cm/sec^2)	3.13(3.11,3.18)
frictional ratio	1.38(1.38,1.40)
molecular weight (kilodalton)	413.5(408.5,415.9)
molecular weight (theor.) (kilodalton)	447.5

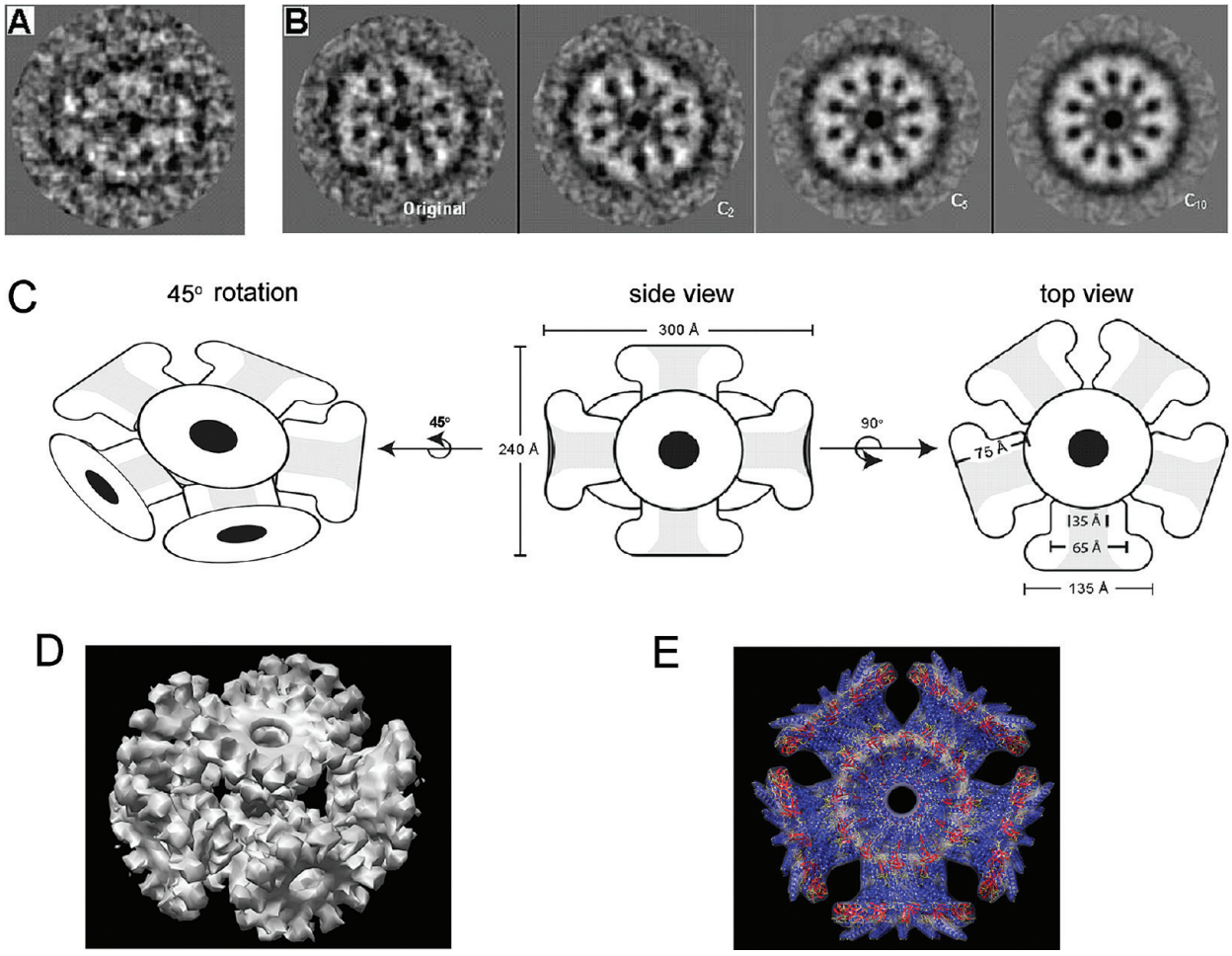

Figure 7. Structure and stoichiometry of ellipsoid nanoparticles from rotational symmetry analysis of TEM salt-embedded sample: (A) side-view of a single nanoparticle from stain-embedding preparations with both orthogonal 2-fold symmetry elements evident; (B) imposition of n-fold rotaional symmetry, with $n = 2$, 5, and 10 (C_2, C_5 and C_{10}) onto a single ellipsoid nanoparticle projection. The 5-fold and 10-fold imposed images closely mimic their parent. However, the 5-fold imposition reveals clear separation between pairs of radial densities which are apparent in the original raw image. (C) Based on the dimension and symmetry assessment, the cartoon representation of an ellipsoid nanoparticle rotated in different view. (D, E) Computer modeling of the ellipsoid nanoparticle in different rotation.

Addition of a C-Terminal Tag Did Not Interfere with the Formation of the Ellipsoid Nanoparticle. The data described above suggests that the ellipsoid nanoparticle contains seven connectors that comprise a total of 84 gp10 molecules whose C-termini protrude from the nanoparticles. That is, the surface of the ellipsoid particle displayed 84 carboxyl groups. If these groups were used for conjugation, each particle would hold up to 84 markers, thus significantly enhancing the detection signals. However, it is important that the protein is able to refold to its original structure after modification, for example, the addition of a peptide to the C-terminus. To determine the possibility of C-terminal conjugation, a tag that binds streptavidin was fused to the C-terminus of each gp10 subunit (termed 'C-Strep'). Our results, derived from TEM imaging and glycerol gradient sedimentation (Figure 2 and 3), demonstrated that the addition of the Strep-tag to the C-terminus of the connector proteins neither interfered with connector assembly nor hindered the formation of the ellipsoid nanoparticle, which suggests that adding biomarkers or fluorescent markers to the surface of the nanoparticle is feasible. However, without the N-terminal extension, the C terminal extension alone did not lead to the formation of the ellipsoid particles.

DISCUSSION

In this study, we found that adding an N-terminal extended tag to the connector promotes the assembly of new ellipsoid nanoparticles that differ in size, shape, and geometry from the original cone-shaped connector. Glycerol gradient sedimentations, TEM, and analytical ultracentrifugation revealed that the new structure is composed of seven connectors, or 84 gp10 proteins. The connectors are arranged with the narrow N-terminus oriented toward the center of the particle and the wider C-terminus exposed at the surface. Removing the N-terminal extended tag reversibly converted the ellipsoid nanoparticle structures back into individual connectors. Although more studies are needed to determine the specific requirement of peptide sequence and length to facilitate nanoparticle formation, it is inferred that the col-

lective N-terminal extensions, and not C-terminal extensions alone, account for the assembly of globular particles. It has been reported in previous studies that native connectors were able to form the nanoparticle structure in the presence of phi29 procapsid pRNA.[12,21,22] What is the driving force that promotes the assembly of the nanoparticles? We believe that both electrostatic and aromatic interactions between the N-terminal extended sequences are responsible for this structural transition. The amino acids in the peptide tag are predominantly acidic or basic, and contain aromatic amino acids.[31−34] Since the N-terminus of the connector is located at the narrow end of the portal vertex, charge−charge and aromatic interactions favor the formation of a compact particle. Formation of particles with 84 amendable, surface-exposed C-termini offers significant potential for the amplification of signals or markers for pathogen detection and the diagnosis of diseases.

MATERIALS AND METHODS

Construction of Plasmid Coding for Re-engineered gp10-Proteins. Two mutant connectors, N-Strep connector and C-strep connector, have been constructed following the method described before.[12] The corresponding plasmids were constructed by inserting the modified gp10 gene into the *Nde* I−*Xho* I sites of the plasmid vector pET-21a(+)[35] (EMB Biosciences, Madison, WI). PCR was used to amplify the gp10 gene from the phi29 genomic DNA-gp3. For plasmid pGp10-NStrep, the Strep-II tag was incorporated to the N-terminus of the gp10 by using the primer pair P1/P2 (Table 3). The plasmid pGp10-CStrep was constructed by a two-step PCR (Table 3). The first PCR, which produced a 5-Gly-linker from the primer pair P3/P4, served as the template for the second PCR and a Strep-II tag was added to the C-terminus by P3/P5 primer pairs. The resulting plasmids, pGp-NStrep and pGp10-CStrep, were confirmed with restriction mapping and sequencing.

Expression and Purification of Connectors and Nanoparticles. The plasmids pGp10-NStrep and pGp10-CStrep were transformed into the *E. coli* strain HMS174 (DE3). Luria−Bertani (LB) medium containing 100 μg/mL ampicillin and induction with 0.5 mM IPTG were employed for cell growth and protein expression as previously described.[36]

Purification of N-Strep connector and C-strep connector was conducted with one step affinity chromatography by Strep-Tactin (IBA, GmbH, Germany).[25] Collected cells were resuspended with Buffer W (100 mM Tris-HCl, pH 8.0, 500 mM NaCl, 1 mM EDTA, 15% glycerol,) and 10−20 column volume (CV) of the clarified lysate was loaded to Strep-Tactin Sepharose resin. After washing the column with Buffer W, Buffer E (15% glycerol, 500 mM NaCl, 1 mM EDTA, 2.5 mM desthiobiotin, 100 mM Tris-HCl, pH 8.0) was used to elute the protein from the column.

Removal of N-Terminal Peptides by Proteinase TEV Cleavage. Cleavage of the N-terminal extensions of the N-strep connector by tobacco etch virus (TEV) protease was achieved by incubating His-TEV with the desired protein at a mass ratio of 1:20 in a solution containing 1 mM DTT. Confirmation of tag removal was conducted by examining samples on 10% SDS-PAGE and 15−35% glycerol gradient sedimentation.

15−35% Glycerol Gradient Sedimentation. Gradient sedimentation with 15−35% glycerol was used to separate the ellipsoid nanoparticles from free connectors. Fractions were collected from the bottom of the sedimentation gradient; particles with higher MW were present in the earliest fractions. After analyzing the samples by SDS-PAGE and silver-staining, the distribution of proteins in each fraction was plotted.

Electron Microscopy Imaging. Copper grids were coated with 400-mesh Formvar and carbon, and the glow was discharged prior to use. Purified protein samples were dialyzed and diluted, when necessary, before negative staining with 2% uranyl acetate. The samples were imaged with a Philips CM-100 TEM operating at 80 kV. CCD readout magnifications were either 39000× or 52000× for ellipsoid nanoparticles or connector particles, respectively. For the projection image analysis, images were collected on a JEOL-JEM2100 at 200 kV. Particles were embedded with 16% ammonium molybdate to prevent drying distortions. Micrographs were then screened to avoid image exhibiting astigmatism, drift, or charging in the analysis.

Analytical Ultracentrifugation (AUC) to Determine the Sedimentation Coefficient As Well As the Shapes and Sizes of the Particles. Purified proteins, C-strep connectors, and N-Strep connectors were studied by sedimentation velocity (SV) experiments performed in a Beckman XLA (Center for Analytical Ultracentrifugation of Macromolecular Assemblies, CAUMA, University of Texas Health Science at San Antonio, UTHSCSA) using absorbance optics measured at 230 nm (N-Strep connector: 0.70 OD, C-strep connector: 1.43 OD). The experiments were performed at 20 °C in 2-channel Epon centerpieces at 20*k* rpm in an AN60 TI rotor using a buffer containing 100 mM Tris, 500 mM NaCl, and 1 mM EDTA. All data were analyzed with the UltraScan software.[26,37] Finite element simulations of the Lamm equation[28] were performed according to methods described by Cao and Demeler.[38] Hydrodynamic corrections were made on the basis of the known buffer composition, while partial specific volume was estimated on the basis of the peptide sequence,[39] as implemented in UltraScan. All SV data were processed as follows: a preliminary van Holde−Weischet analysis was used to obtain a model-independent and diffusion-corrected range for the sedimentation coefficients of each sample;[27] the value of the range was used to initialize a 2-dimensional spectrum analysis (2DSA).[40] Simultaneously, all systematic noise was removed from this data.[41] All subsequent analyses were performed on modified data sets that had all time-invariant contributions subtracted. After subtraction of time-invariant noise, the van Holde−Weischet analysis was repeated using the refined data (see Figure 4 for a combined integral distribution plot). Afterward, 1.5% of the boundary values were excluded from the top and the bottom of the boundary to eliminate potential stochastic noise contributions. Further refinement of the time-invariant noise corrected data was achieved by performing a 2DSA Monte Carlo (MC) analysis with 50 iterations. This method attenuates stochastic noise contributions to the solution by enhancing the intrinsic signal through signal amplification.[30] The resulting data were used to initialize the genetic algo-

TABLE 3. Primer Sequence for the Construction of gp10 Vectors

location of extension	primer	primer sequence (5′−3′)
N-terminus	P1	CGTAACCTGCATATGTGGAGCCACCCGCAGTTCGAAAAGGATTATGATATCCCTACGAC
	P2	CTAGCTATCTCGAGCTACTACTCATTTGTTTCACCGTCC
C-terminus	P3	CGCAGCTGGCATATGGCACGTAAACGCAGTAAC
	P4	GGATGACTCCAACCTCCTCCACCACCTCCCTCATTTGTTTCACCGT
	P5	ATAATGTTCTCGAGCTACTTTTCGAACTGCGGATGACTCCAACCTC

rithm analysis (GA).[42] This method accomplishes a parsimonious regularization, satisfying Occam's razor (a process that will find the most parsimonious solution, *i.e.*, a solution with the fewest parameters that still produce the lowest possible residual mean square deviation in the data fit).[29] A GA−MC analysis of the parsimonious solution was used to obtain confidence intervals for molecular weight, frictional ratio, sedimentation and diffusion coefficients, and partial concentration. All computations were performed on the TIGRE cluster at the Bioinformatics Core Facility at UTHSCSA and the Texas Advanced Computing Center at the University of Texas in Austin (TACC).

Acknowledgment. We thank Karen Rufus from Vanderbilt University for providing the TEV proteinase expressing strains, Debra Sherman from Purdue University for EM imaging, Anne Vonderheide from University of Cincinnati for valuable comments, and Virgil Schirf (UTHSCSA) for assistance with the analytical ultracentrifugation experiments at CAUMA. The research was mainly supported by NIH grants EB003730 (P.G.), GM59944 (P.G.), and by EY018230 "NIH Nanomedicine Development Center: Phi29 DNA packaging Motor for Nanomedicine (P.G.)". The development of the UltraScan software is supported by NIH Grant RR022200 (B.D.). We thank the staff at TACC for support and acknowledge NSF Teragrid Allocation TG-MCB070038 (B.D.).

Note added after ASAP publication: The original Web version of this paper published on July 17, 2009 was corrected for two numerical values, a unit designation, and a reference citation, and the paper was reposted on the Web July 27, 2009.

REFERENCES AND NOTES

1. Niemeyer, C. M. Nanoparticles, Proteins, and Nucleic Acids: Biotechnology Meets Materials Science. *Angew. Chem., Int. Ed.* **2001**, *40*, 4128–4158.
2. Seeman, N. C. DNA In A Material World. *Nature* **2003**, *421*, 427–431.
3. Guo, P. RNA Nanotechnology: Engineering, Assembly, and Applications in Detection, Gene Delivery, and Therapy. *J. Nanosci. Nanotechnol.* **2005**, *5*, 1964–1982.
4. Rothemund, P. W. K. Folding DNA to Create Nanoscale Shapes and Patterns. *Nature* **2006**, *440*, 297–302.
5. Shu, D.; Moll, D.; Deng, Z.; Mao, C.; Guo, P. Bottom-Up Assembly of RNA Arrays and Superstructures as Potential Parts in Nanotechnology. *Nano Lett.* **2004**, *4*, 1717–1724.
6. Chworos, A.; Severcan, I.; Koyfman, A. Y.; Weinkam, P.; Oroudjev, E.; Hansma, H. G.; Jaeger, L. Building Programmable Jigsaw Puzzles with RNA. *Science* **2004**, *306*, 2068–2072.
7. Shu, D.; Huang, L.; Hoeprich, S.; Guo, P. Construction of Phi29 DNA-Packaging RNA (pRNA) Monomers, Dimers, and Trimers with Variable Sizes and Shapes as Potential Parts for Nano-Devices. *J. Nanosci. Nanotechnol.* **2003**, *3*, 295–302.
8. Zhang, F.; Lemieux, S.; Wu, X.; St.-Arnaud, S.; McMurray, C. T.; Major, F.; Anderson, D. Function of Hexameric RNA in Packaging of Bacteriophage Phi29 DNA *in vitro*. *Mol. Cell.* **1998**, *2*, 141–147.
9. Guo, P.; Zhang, C.; Chen, C.; Trottier, M.; Garver, K. Inter-RNA Interaction of Phage Phi29 pRNA to Form a Hexameric Complex for Viral DNA Transportation. *Mol. Cell* **1998**, *2*, 149–155.
10. Perez, J. M.; Simeone, F. J.; Saeki, Y.; Josephson, L.; Weissleder, R. Viral-Induced Self-Assembly of Magnetic Nanoparticles Allows the Detection of Viral Particles in Biological Media. *J. Am. Chem. Soc.* **2003**, *125*, 10192–10193.
11. Mao, C.; Flynn, C. E.; Hayhurst, A.; Sweeney, R.; Qi, J.; Georgiou, G.; Iverson, B.; Belcher, A. M. Viral Assembly of Oriented Quantum Dot Nanowires. *Proc. Natl. Acad. Sci. U.S.A.* **2003**, *100*, 6946–6951.
12. Guo, Y.; Blocker, F.; Xiao, F.; Guo, P. Construction and 3-D Computer Modeling of Connector Arrays with Tetragonal to Decagonal Transition Induced by pRNA of Phi29 DNA-Packaging Motor. *J. Nanosci. Nanotechnol.* **2005**, *5*, 856–863.
13. Xiao, F.; Sun, J.; Coban, O.; Schoen, P.; Wang, J. C.; Cheng, R. H.; Guo, P. Fabrication of Massive Sheets of Single Layer Patterned Arrays Using Re-engineered Phi29 Motor Dodecamer. *ACS Nano* **2009**, *3*, 100–107.
14. Moll, D.; Huber, C.; Schlegel, B.; Pum, D.; Sleytr, U. B.; Sara, M. S-Layer-Streptavidin Fusion Proteins as Template for Nanopatterned Molecular Arrays. *Proc. Natl. Acad. Sci. U.S.A.* **2002**, *99*, 14646–14651.
15. Sára, M.; Pum, D.; Schuster, B.; Sleytr, U. B. S-Layers as Patterning Elements for Application in Nanobiotechnology. *J. Nanosci. Nanotechnol.* **2005**, *5*, 1939–1953.
16. Sleytr, U. B.; Sara, M. Bacterial and Archaeal S-Layer Proteins: Structure−Function Relationships and Their Biotechnological Applications. *Trends Biotechnol.* **1997**, *15*, 20–26.
17. Gentilucci, L.; Tolomelli, A.; Squassabia, F. Peptides and Peptidomimetics in Medicine, Surgery and Biotechnology. *Curr. Med. Chem.* **2006**, *13*, 2449–2466.
18. Guo, P.; Grimes, S.; Anderson, D. A Defined System for *in Vitro* Packaging of DNA-gp3 of the Bacillus Subtilis Bacteriophage Phi29. *Proc. Natl. Acad. Sci. U.S.A.* **1986**, *83*, 3505–3509.
19. Simpson, A. A.; Leiman, P. G.; Tao, Y.; He, Y.; Badasso, M. O.; Jardine, P. J.; Anderson, D. L.; Rossman, M. G. Structure Determination of the Head−Tail Connector of Bacteriophage Phi29. *Acta Crystallogr.* **2001**, *D57*, 1260–1269.
20. Guasch, A.; Pous, J.; Ibarra, B.; Gomis-Ruth, F. X.; Valpuesta, J. M.; Sousa, N.; Carrascosa, J. L.; Coll, M. Detailed Architecture of a DNA Translocating Machine: The High-Resolution Structure of the Bacteriophage Phi29 Connector Particle. *J. Mol. Biol.* **2002**, *315*, 663–676.
21. Tsuprun, V.; Anderson, D.; Egelman, E. H. The Bacteriophage Phi29 Head−Tail Connector Shows 13-Fold Symmetry in Both Hexagonally Packed Arrays and as Single Particles. *Biophys. J.* **1994**, *66*, 2139–2150.
22. Garver, K.; Guo, P. Boundary of pRNA Functional Domains and Minimum pRNA Sequence Requirement for Specific Connector Binding and DNA Packaging of Phage Phi29. *RNA* **1997**, *3*, 1068–1079.
23. Maier, T.; Drapal, N.; Thanbichler, M.; Bock, A. Strep-Tag II Affinity Purification: An Approach to Study Intermediates of Metalloenzyme Biosynthesis. *Anal. Biochem.* **1998**, *259*, 68–73.
24. Voss, S.; Skerra, A. Mutagenesis of a Flexible Loop in Streptavidin Leads to Higher Affinity for the Strep-Tag II Peptide and Improved Performance in Recombinant Protein Purification. *Protein Eng.* **1997**, *10* (8), 975–982.
25. Schmidt, T. G. M.; Skerra, A. The Strep-Tag System for One-Step Purification and High-Affinity Detection or Capturing of Proteins. *Nat. Protoc.* **2007**, *2*, 1528–1535.
26. Brookes, E.; Demeler, B. Parallel Computational Techniques for the Analysis of Sedimentation Velocity Experiments in Ultrascan. *Colloid Polym. Sci.* **2008**, *286*, 139–148.
27. Demeler, B.; van Holde, K. E. Sedimentation Velocity Analysis of Highly Heterogeneous Systems. *Anal. Biochem.* **2004**, *335*, 279–288.
28. Lamm, O. Die Differentialgleichung der Ultrazentrifugierung. *Ark. Mat. Astr. Fys.* **1929**, *21B*, 1–4.
29. Brookes, E.; Demeler, B. Parsimonious Regularization Using Genetic Algorithms Applied to the Analysis of Analytical Ultracentrifugation Experiments. In *GECCO Proceedings*, ACM 978-1-59593-697-1/07/0007, **2007**.
30. Demeler, B.; Brookes, E. Monte Carlo Analysis of Sedimentation Experiments. *Colloid Polym. Sci.* **2008**, *286*, 129–137.
31. Burley, S. K.; Petsko, G. A. Aromatic−Aromatic Interaction—A Mechanism of Protein-Structure Stabilization. *Science* **1985**, *229*, 23–28.
32. Tewari, A. K.; Dubey, R. Emerging Trends in Molecular Recognition: Utility of Weak Aromatic Interactions. *Bioorg. Med. Chem.* **2008**, *16*, 126–143.

33. Blakaj, D. M.; McConnell, K. J.; Beveridge, D. L.; Baranger, A. M. Molecular Dynamics and Thermodynamics of Protein-RNA Interactions: Mutation of a Conserved Aromatic Residue Modifies Stacking Interactions and Structural Adaptation in the U1A-Stem Loop 2 RNA Complex. *J. Am. Chem. Soc.* **2001**, *123*, 2548–2551.
34. Shiels, J. C.; Tuite, J. B.; Nolan, S. J.; Baranger, A. M. Investigation of a Conserved Stacking Interaction in Target Site Recognition by the U1A Protein. *Nucleic Acids Res.* **2002**, *30*, 550–558.
35. Studier, F. W.; Rosenberg, A. H.; Dunn, J. J.; Dubendorff, J. W. Use of T7 RNA Polymerase to Direct the Expression of Cloned Genes. *Methods Enzymol.* **1990**, *185*, 60–89.
36. Guo, P.; Moss, B. Interaction and Mutual Stabilization of the Two Subunits of Vaccinia Virus Mrna Capping Enzyme Co-Expressed in *Escherichia Coli*. *Proc. Natl. Acad. Sci. U.S.A.* **1990**, *87*, 4023–4027.
37. Demeler, B. A Comprehensive Data Analysis Software Package for Analytical Ultracentrifugation Experiments. In *Modern Analytical Ultracentrifugation: Techniques and Methods*; Scott, D. J., Harding, S. E., Rowe, A. J. Eds.; Royal Society of Chemistry: U.K. 2005; pp 210−229.
38. Cao, W. M.; Demeler, B. Modeling Analytical Ultracentrifugation Experiments with an Adaptive Space−Time Finite Element Solution of the Lamm Equation. *Biophys. J.* **2005**, *89*, 1589–1602.
39. Durchschlag, H. *Thermodynamic Data for Biochemistry and Biotechnology*; Springer-Verlag, New York, 1986.
40. Brookes, E.; Boppana, R. V.; Demeler, B. Computing Large Sparse Multivariate Optimization Problems with an Application in Biophysics. *Supercomputing '06*, ACM 0-7695-2700-0/06 **2006**.
41. Schuck, P.; Demeler, B. Direct Sedimentation Analysis of Interference Optical Data in Analytical Ultracentrifugation. *Biophys. J.* **1999**, *76*, 2288–2296.
42. Brookes, E.; Demeler, B. Analytical Ultracentrifugation VIII. In *Progress in Colloid Polymer Science*, Wandrey, C., Colfen, H., Eds.: Springer, New York, 2006; pp 78−82.